Acta Geophysica (2021) 69:821–839
https://doi.org/10.1007/s11600-021-00573-x

RESEARCH ARTICLE - APPLIED GEOPHYSICS

Using total variation method to estimate the permeability model of a gas-fingering area in an Iranian carbonate reservoir

Mohammad Hosseini[1]

Received: 29 August 2020 / Accepted: 13 March 2021 / Published online: 1 April 2021
© Institute of Geophysics, Polish Academy of Sciences & Polish Academy of Sciences 2021

Abstract

A dozen of inversion methods are applied and tested to estimate the permeability of the area where gas-fingering event has taken place in an Iranian carbonate reservoir located southwest of Iran. In a previous work, the gas-fingering event was detected by inverting the 3D seismic data and in this study the permeability model in that area is estimated. Because the lateral area of the gas-fingering event is narrow, the whole system conducting the injected gas can be considered as one rock unit system and therefore the assumption of horizontal linear steady-state flow can be applied. Inversion methods are exploited to determine the permeability in the interval of interest. The interval of interest is located at the crest and involves four wells among which one is the gas-injection well. To investigate the feasibility of such an approach and select the best possible inversion method, first a controlled experiment for the system is designed and studied. The porosity values of the system are known from seismic data inversion and the permeability values are the desired parameters. The permeability values at well locations are known via well-test data and are used as constraints in the inversion procedure. The interval of interest is discretized and a simulator is used to simulate the fluid flow in the controlled system in order to apply and validate the inversion methods. All calculations are performed in the MATLAB environment. According to the results from the controlled experiment, the Maximum Entropy and Total Variation methods were found to be the best two inversion methods which were successful in retrieving the true permeability model. Similar comparative study using different inversion methods is performed for the real case for which the results retrieved by the Total Variation method is most reliable as it suggests the best recovery of the permeability value for the check-well. An estimation of the fracture permeabilities for the area under study also indicated that the inverted permeability values are most representing the fracture permeabilities rather than the matrix. The results of this study will be used to tune the field simulation model in terms of rock and fluid properties, consider the inverted permeability model as further constraints for the reservoir history-matching of the oil field, reconsider the factors involving the gas injection plan for the oil field, and obtain insights for further field development plans in other nearby oil fields.

Keywords Total variation method · Tikhonov regularization method · Conjugate gradient least squares method · Maximum entropy method · Gas-fingering feature · Permeability estimation

Introduction

History-matching is a highly nonlinear inverse problem and the scientists working in the area of petroleum engineering have taken different approaches to deal with this problem. There is a high interest in the subject not only because the case of reservoir management and decision-making is very important economically but also because the scientific approach to solve the subject is very challenging. Solving the reservoir history-matching problem as an inversion procedure involves high nonlinearity, because a big number of parameters contribute to the fluid flow through porous media, and it is beautiful to deal with such challenging problems.

There is a wide literature and background for methods which are evolved to remediate the inverse problem of reservoir history-matching. Oliver (2010) has reviewed different aspects of the history-matching inverse problem and the

Communicated by Michal Malinowski (CO-EDITOR-IN-CHIEF)/Liang Xiao (ASSOCIATE EDITOR).

✉ Mohammad Hosseini
hosseini.mhmd@yahoo.ca

[1] Geology and Geophysics Department, National Iranian South Oil Company, Ahwaz, Iran

evolution of the approaches until recent. To mention a few, Romero and Carter (2001) and Chakra and Saraf (2016) have taken advantage of the genetic algorithms for reservoir parameterization. Caers and Hoffman (2006) and Aanonsen et al. (2019) have proposed the probability perturbation method in the context of Bayesian inverse modeling for reservoir history-matching.

Reservoir history-matching formulated as a minimization problem include the computation of the derivatives of the objective function with respect to the model variables. One example of such an approach is the utilization of the conjugate gradient algorithm as the inversion method. In the current study, the conjugate gradient method is used as one of the inversion procedures for extracting the reservoir permeability from the production data. The gradient methods are used by Cominelli et al. (2007) for reservoir history-matching; Rodrigues (2006) specifically uses the sensitivity equation method (or the forward method) to perform such task. The adjoint state method is the efficient methodology for accurately computing the gradient of a function of the state variables with respect to the model variables in case of large numbers of model parameters which usually occur in practical history-matching problems. Examples of such applications include the work of Li et al. (2003), Eydinov et al. (2008), and Onwuchekwa et al. (2017). In cases of sufficiently smooth objective function, Gauss–Newton method or its variations, such as Levenberg–Marquardt method, can be used to compute optimal local directions to change the model parameters. Gao et al. (2017a, b) have applied the Gauss–Newton method and Chen and Oliver (2013) and Zhang and Awotunde (2016) have applied Levenberg–Marquardt method for reservoir history-matching.

Another interesting idea which is used for matching the history of the reservoir is the streamline simulation which includes ray tracing and production tomography, as examples of such approaches the reader is referred to Oyerinde et al. (2009) and Kazemi and Stephen (2013). In fact, this approach is a stimulation of the geophysical tomography adapted for reservoir history-matching. An adaptive multiscale version of the streamline simulation is represented by Stenerud et al. (2008). The current study is a one dimensional example of the production tomography.

A new generation of methods was developed in reservoir history-matching in order to quantify the risk and uncertainty in the reservoir management. Markov chain Monte Carlo (MCMC) methods are well suited for the reservoir history-matching problem if the problem is posed as a prior distribution for model variables and a likelihood function for the model variables given the data. In this context, first a reservoir model sampled from the prior distribution is chosen; then at each iteration a new reservoir model is selected and tested. The new reservoir model is discarded if inferior results are obtained and the iteration continues until sufficient number of suitable models are selected. Examples of applying the MCMC approach for reservoir history-matching are Efendiev et al. (2006), Romary (2009), Olalotiti-Lawal and Datta-Gupta (2018), and Liao et al. (2019). Another powerful approach to reservoir history-matching is the utilization of the ensemble Kalman filter (EnKF) method which is a sequential data assimilation method. Data assimilation methods are mostly used in the area of meteorology and its application to reservoir history-matching is developed by Evensen (2009). In this method, both the model variables (e.g., permeability) and state variables (e.g., pressure) are updated. Recent applications of the EnKF method for history-matching include Emerick and Reynolds (2011), Heidari et al. (2011), and Jo et al. (2017), and Raghu et al. (2017).

Other interesting approaches for reservoir history-matching include the work of Gonzalez-Rodriguez et al. (2005) which has used the propagation back-propagation method to solve the history-matching problem in a reservoir and reconstruct the permeability models using the production data. Moreover, Maschio and Schiozer (2008) have used independent objective functions for assisted history-matching to obtain the permeability model of the reservoir using production data. Kazemi and Stephen (2012) have also practiced different schemes of automatic history-matching for reservoir modeling by integrating time-lapse seismic and production data using multi-variable approaches as the updating schemes.

Despite all of the above studies, a work which illustrates the application of the inversion methods and concepts is missing. Of this kind, dos Santos Amorim et al. (2010) has used the Truncated Singular Value Decomposition (TSVD) method to estimate the permeability model of a reservoir using pressure and flow rate data. The TSVD method is one of the methods which is tested in this study. The importance of this study is that it uses different inversion methodologies for a real case gas-fingering event. Four different inversion methods are specifically emphasized in this paper which are discussed in the next section. It explicitly describes the procedure and logically proposes the best inversion method which is able to reconstruct the permeability model of the area under study. An estimation of the fracture permeabilities is also presented. The work steps of the current study are represented in Fig. 1. These steps are explicitly presented and discussed through the paper.

Inversion methods

In many fields of science, dealing with the inverse problems is a common practice. It is always the case that having a set of observation data, $\boldsymbol{d}$, the task is to characterize the properties of the model, $\boldsymbol{m}$. It is common to consider the physics of

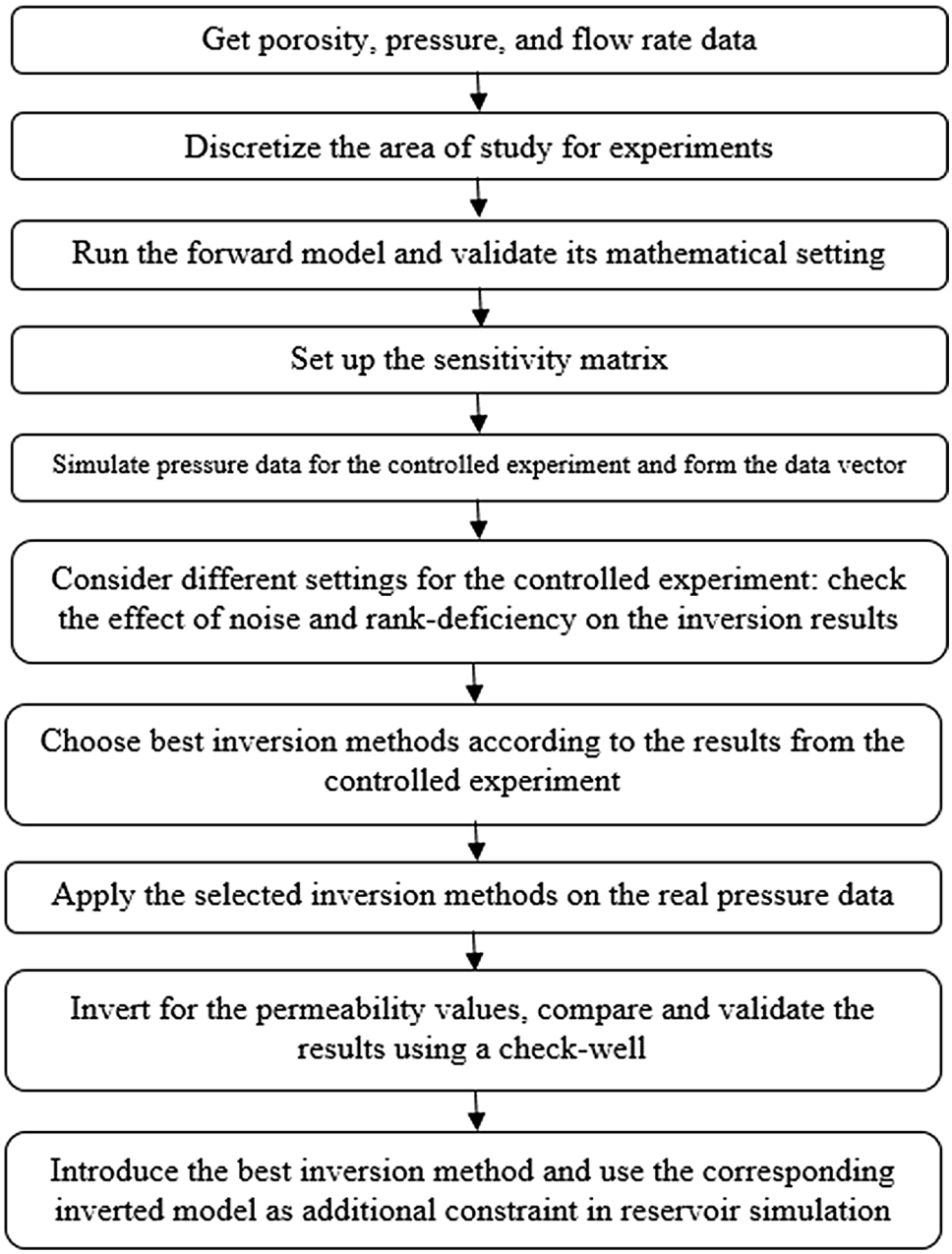


Fig. 1 Work-steps of the current study

the system, G, as a known function or matrix which relates the observations to the model.

A general parameter estimation problem can be written as $G(\boldsymbol{m}) = \boldsymbol{d}$ which suggests that the data $\boldsymbol{d}$ has a nonlinear relationship with $\boldsymbol{m}$ through the nonlinear system G. In the case of linear system of equations, the observation data can be written as $\boldsymbol{d} = G(\boldsymbol{m}) = G\boldsymbol{m}$. The data itself is not perfect and it always contain some amount of noise such that we can write $\boldsymbol{d} = \boldsymbol{d}_{true} + \boldsymbol{\eta} = G\left(\boldsymbol{m}_{true}\right) + \boldsymbol{\eta}$, where $\boldsymbol{\eta}$ represents the noise in the data.

For a parameter estimation problem as posed above, numerous inversion schemes exit. Some of such methods are general and can be applied to any inverse problem; however the reliability of the results are questionable. As a result, special inversion schemes are proposed to handle specific inverse problems by adding additional regularization terms to the system of equations.

For this study, numerous inversion methods were applied which include truncated singular value decomposition (TSVD), Kaczmarz method, *Tikhonov regularization methods* (zero-, first-, and second-order), truncated generalized singular value decomposition (TGSCD), conjugate gradient singular value decomposition (CGSVD), generalized cross-validation (GCV), *conjugate gradient least squares* (CGLS), nonnegative least squares (NNLS), bounded variables least squares (BVLS), *maximum entropy*, and *total variation*

(TV). However, to represent the results, the focus in this paper is on the methods represented below.

Tikhonov regularization methods

One method for stabilizing the solution to inverse problems is the Tikhonov regularization methods. In the zeroth-order approach the consideration is over minimizing $\|\boldsymbol{Gm}-\boldsymbol{d}\|_2^2+\alpha^2\|\boldsymbol{m}\|_2^2$ which is called the damped least squares problem, where α is a regularization parameter. Forming the equations to solve this problem will result in $\left(\boldsymbol{G}^T\boldsymbol{G}+\alpha^2\boldsymbol{I}\right)\boldsymbol{m}=\boldsymbol{G}^T\boldsymbol{d}$ where the solution is $\boldsymbol{m}_\alpha=\sum_{i=1}^{k}\frac{s_i^2}{s_i^2+\alpha^2}\frac{(\boldsymbol{U}_{.i})^T\boldsymbol{d}}{s_i}\boldsymbol{V}_{.,i}$ and $k=\min(m,n)$.

In higher order Tikhonov regularization approaches the attempt basically is to minimize the norm of the first or second derivative of the model, $\boldsymbol{m}$. In other words some roughness matrices, denoted by $\boldsymbol{L}$, are used in order to minimize $\|\boldsymbol{Gm}-\boldsymbol{d}\|_2^2+\|\boldsymbol{Lm}\|_2^2$. This approach is the first-order and second-order Tikhonov regularization method if $\boldsymbol{Lm}$ is the finite-difference approximation proportional to the first and second derivative of the model, $\boldsymbol{m}$, respectively. In this case, the solution will be

$$\boldsymbol{m}_{\alpha,L}=\boldsymbol{G}^{\#}\boldsymbol{d}\ \text{where}\ \boldsymbol{G}^{\#}=\left(\boldsymbol{G}^T\boldsymbol{G}+\alpha^2\boldsymbol{L}^T\boldsymbol{L}\right)^{-1}\boldsymbol{G}^T \tag{1}$$

For More details the reader is referred to Aster et al. (2005).

Conjugate gradient least squares method

In the conjugate gradient least squares (CGLS) method, the least squares problem $min\|\boldsymbol{Gm}-\boldsymbol{d}\|_2$ is solved by applying the conjugate gradient algorithm to the normal equations $\boldsymbol{G}^T\boldsymbol{Gm}=\boldsymbol{G}^T\boldsymbol{d}$. The CGLS algorithm is given as following.

Given a system of equations $\boldsymbol{Gm}=\boldsymbol{d}$, let $k=0$, $\boldsymbol{m_0}=\boldsymbol{0}$, $\boldsymbol{p_{-1}}=\boldsymbol{0}$, $\beta_0=0$, $\boldsymbol{s}_0=\boldsymbol{d}$, and $\boldsymbol{r_0}=\boldsymbol{G}^T\boldsymbol{s_0}$. Repeat the following iterations until convergence.

1. If $k>0$, let $\beta_k=\frac{\boldsymbol{r}_k^T\boldsymbol{r}_k}{\boldsymbol{r}_{k-1}^T\boldsymbol{r}_{k-1}}$.
2. Let $\boldsymbol{p}_k=\boldsymbol{r}_k+\beta_k\boldsymbol{p}_{k-1}$.
3. Let $\alpha_k=\frac{\boldsymbol{r}_k^T\boldsymbol{r}_k}{(\boldsymbol{Gp}_k)^T(\boldsymbol{Gp}_k)}$.
4. Let $\boldsymbol{x}_{k+1}=\boldsymbol{x}_k+\alpha_k\boldsymbol{p}_k$.
5. Let $\boldsymbol{s}_{k+1}=\boldsymbol{s}_k-\alpha_k\boldsymbol{Gp}_k$.
6. Let $\boldsymbol{r}_{k+1}=\boldsymbol{G}^T\boldsymbol{s}_{k+1}$.
7. Let $=k+1$.

Maximum entropy method

In the maximum entropy method, a regularization function of the form $\sum_{i=1}^{n}m_i\ln\left(w_im_i\right)$ is used in which w_i are a set of positive weights. This method is used for the type of problems where the model parameters are considered to be positive values.

In the maximum entropy regularization approach, the entropy of model $\boldsymbol{m}$ is maximized subject to a constraint on the size of the misfit $\|\boldsymbol{Gm}-\boldsymbol{d}\|_2$ in the following sense:

$$\begin{aligned}\max\ &-\sum_{i=1}^{n}m_i\ln\left(w_im_i\right)\\ &\|\boldsymbol{Gm}-\boldsymbol{d}\|_2\le\delta\\ &\boldsymbol{m}\ge 0\end{aligned} \tag{2}$$

Using a Lagrange multiplier, Eq. (2) can be written as the following:

$$\begin{aligned}\min\ &\|\boldsymbol{Gm}-\boldsymbol{d}\|_2^2+\alpha^2\sum_{i=1}^{n}m_i\ln\left(w_im_i\right)\\ &\boldsymbol{m}\ge 0\end{aligned} \tag{3}$$

Total variation method

The Total Variation (TV) method is appropriate for models with discontinuous jumps. The TV regularization function can be written as

$$TV(\boldsymbol{m})=\sum_{i=1}^{n-1}\left|m_{i+1}-m_i\right|=\|\boldsymbol{Lm}\|_1 \tag{4}$$

where $\boldsymbol{L}$ is a discretization of the gradient operator.

A solution to the TV regularization problem would be to pose the misfit function, $\|\boldsymbol{Gm}-\boldsymbol{d}\|_2$, as an L_1 regularization problem under the following scheme:

$$\min\|\boldsymbol{Gm}-\boldsymbol{d}\|_1+\alpha\|\boldsymbol{Lm}\|_1 \tag{5}$$

This can be written as

$$\min\left\|\begin{bmatrix}\boldsymbol{G}\\ \alpha\boldsymbol{L}\end{bmatrix}m-\begin{bmatrix}\boldsymbol{d}\\ 0\end{bmatrix}_1\right\| \tag{6}$$

which can be solved using iteratively reweighted least squares (IRLS) method.

Field and data description

The reservoir under study is the Asmari Formation from an oil field located southwest of Iran. The reservoir is an anticline located in the Zagros sedimentary basin and is discovered in 1962. The gas injection into the reservoir is started in the year of 2005 from well No. 8 for the purpose of pressure maintenance. The study discharged by Hosseini and Riahi (2019b) detected the gas-fingering event by inverting the 3D seismic data recorded during the years of 2009 and 2010, Fig. 2. According to pressure data collected from the reservoir, the pressure is lifted at nearby wells.

In this paper, the area of interest is the portion of reservoir around the injection well No. 08 which include wells No. 01, 09, and 02. These latter wells are not on production to avoid gas production, however, they are used for the purpose of pressure monitoring. The problem at hand would be to infer the permeability values for the gas-fingering area using the injection rate and pressure data at the injection well and the pressure data at the monitoring wells. Figure 3a indicates the spectral decomposition profile of the depth of interest from the Asmari Formation and Fig. 3b is the same profile with the well locations overlaid.

Inversion of the seismic data (Hosseini and Riahi 2019b) has resulted in extracting the porosity map which is indicated in Fig. 4a. The porosity profile extracted for the area under study is represented in Fig. 3b. Also, the real permeability values at the well locations are known from the well-test data to be 627, 511, 490, and 688 millidarcies for wells No. 01, 08, 09, and 02, respectively. The permeability

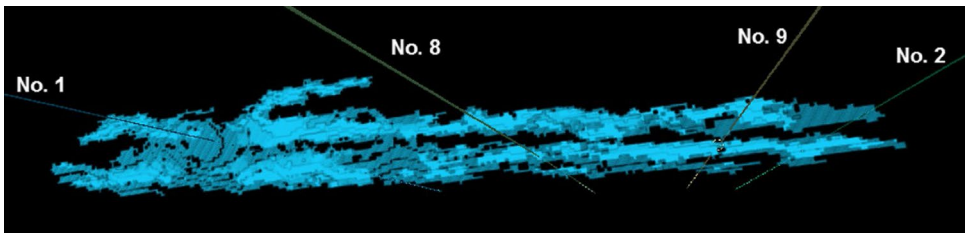


Fig. 2 The gas injection interval (Hosseini and Riahi 2019b)

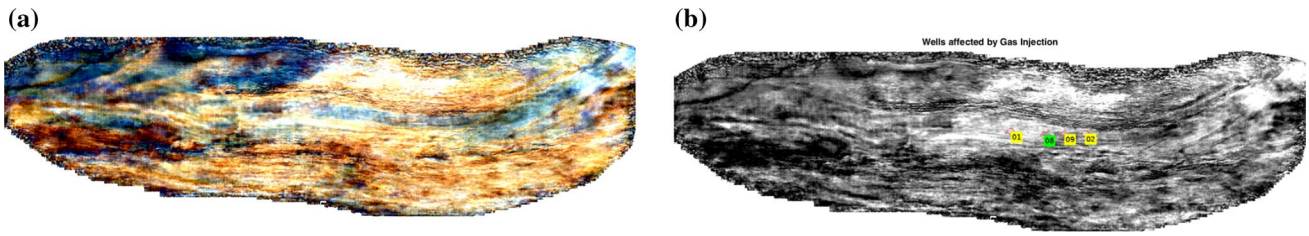


Fig. 3 **a** The image of spectral decomposition profile for the horizon of interest (Hosseini and Riahi 2019a); **b** same, overlaid by the wells in the gas-fingering interval

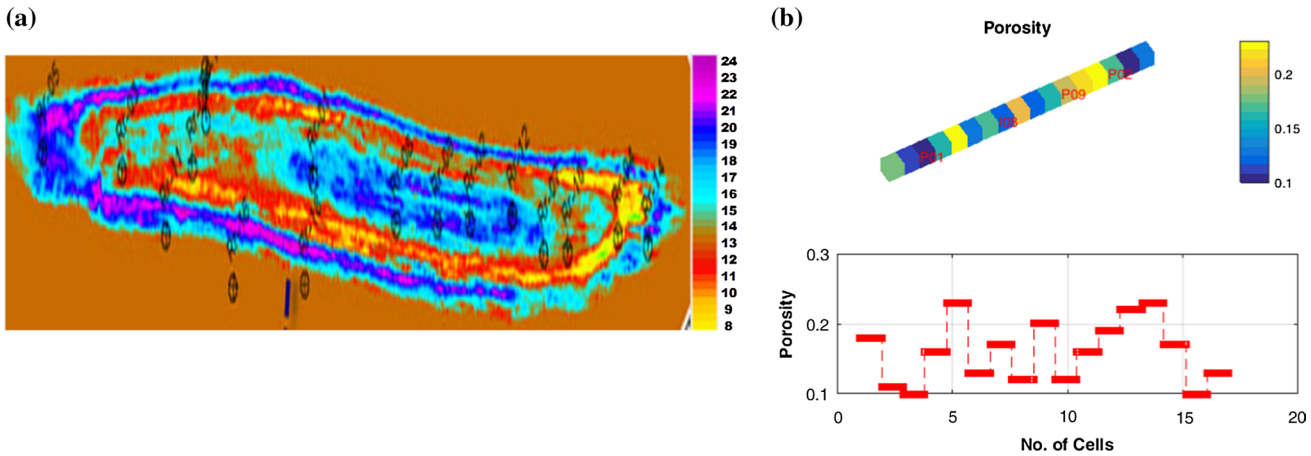


Fig. 4 **a** The porosity map of the field; **b** the porosity profile extracted for the area under study

values represent both matrix and fracture permeabilities of the specified location, indeed.

The pressure data are recorded, except for the injection well (i.e., well No. 08), six months after the injection began as depicted in Fig. 5a. The data are not recorded in uniform fashion due to operational issues. Few outliers are also discarded from the plots and hence from the inversion procedure. The injection rate data is also illustrated in Fig. 5b. The injection rate data at each point represents the average of the rate over the period of 30 days, i.e., the time step for the simulation model. The four considerable drops of the rate, which is observable on the history plot, are due to specifying the gas for domestic consumption in cold seasons of the year.

The initial pressure of the reservoir, i.e., before production, was measured to be 3600 psi. Well No. 8 is completed by a $9\frac{5}{8}$ inch diameter casing. The flow rate of the injected gas, i.e., well No. 08, is kept at around 250 RB/D. The gas injection rate is converted from CuFt/D to RB/D for dimension consistency in the forward and backward modeling schemes. Reservoir production data are measured at an interval of 30 days which is considered as the time step. Wells 01, 09, and 02 are not on production but the pressure data are recorded at these locations. Gas injection process is started

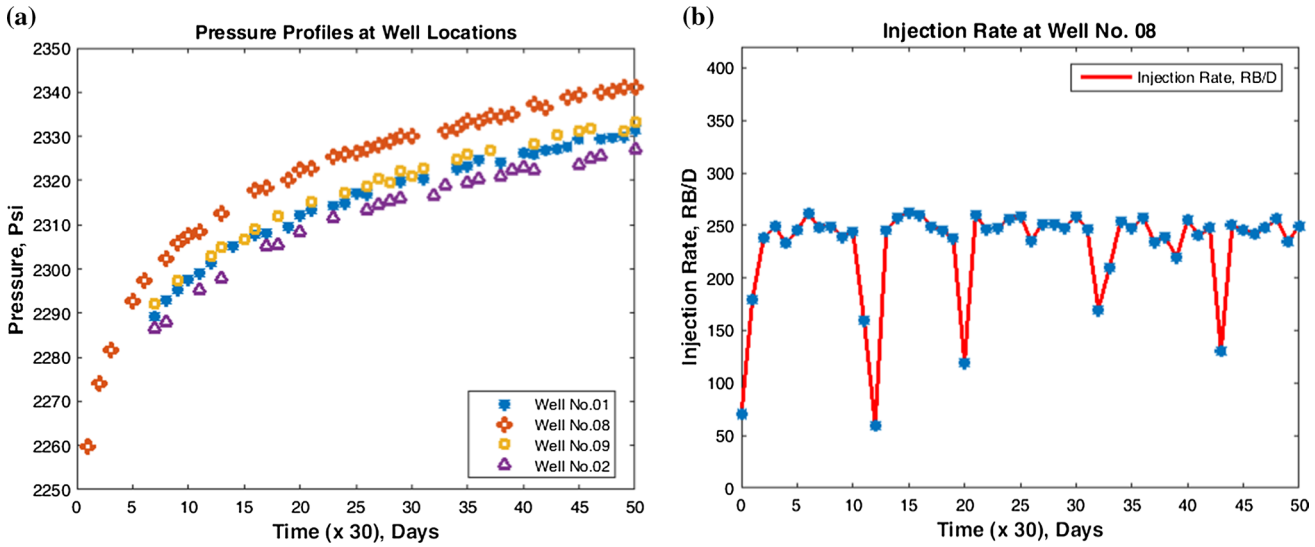


Fig. 5 **a** The pressure data; **b** the injection rate

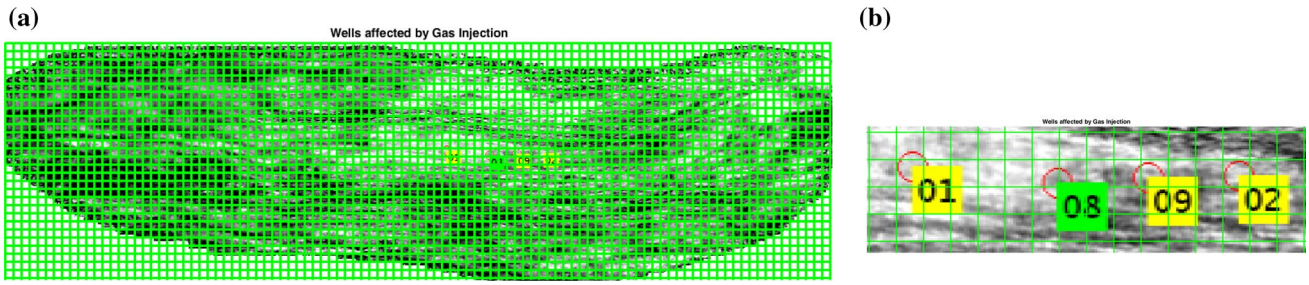


Fig. 6 **a** Simulation grid overlaid on the studied reservoir; **b** a zoom of the area of interest

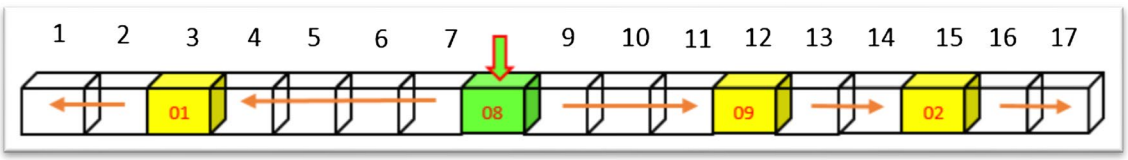


Fig. 7 Scheme for the discretization of the problem for the area of interest

in 2005 and the seismic data is recorded during the year of 2009 to 2010. For this study we are only interested in the first five years of the reservoir behavior and the gas injection history, because it is the time that the gas injection process is started at well No. 08 until the time of recording the seismic data. Therefore, an approximate span of 1500 days is considered for the inversion of pressure data. The problem is discretized according to Figs. 6, 7 and a grid volume of $250 \times 12 \times 80$ cubic feet is considered for the cells. The gas viscosity is 0.15 centipoise and the total compressibility is approximated to be 3×10^{-6}. The effect of skin factors are neglected in the problem setting.

Setting of the problem

Forward modeling

Having all the above reservoir data a forward model has to be set up in order to calculate pressure in each cell at each time. The finite-difference equations for one-dimensional single-phase flow, as the forward model equations, can be obtained from the differential equation as

$$C_1 \frac{\partial}{\partial x}\left(\frac{k(x)A}{\mu}\frac{\partial p(x,t)}{\partial x}\right) - q\delta\left(x - x_0\right) = C_2\phi(x)c_t A\frac{\partial p(x,t)}{\partial t} \text{ for } 0 < x < L \text{ and } t > 0 \tag{7}$$

and

$$\frac{\partial p(0,t)}{\partial x} = \frac{\partial p(L,t)}{\partial x} = 0, \text{ for all } t > 0 \tag{8}$$

and

$$(x,0) = p_{\text{in}}, \text{ for all } t > 0 \tag{9}$$

where Eqs. (8) and (9) are the boundary conditions for Eq. (7). In Eq. (7), the Dirac delta function, $\delta\left(x - x_0\right)$, is used to model a production or injection well at location x_0 by a rate of q (Oliver et al. 2008).

Discretizing For the spatial and time derivatives, the following finite-difference equations are obtained (Ertekin et al. 2001; Kreyszig 2006; Oliver et al. 2008; Quarteroni et al. 2000)

$$C_1\frac{k_{i+\frac{1}{2}}A}{\mu}\left(\frac{p_{i+1}^n - p_i^n}{\Delta x}\right) - C_1\frac{k_{i-\frac{1}{2}}A}{\mu}\left(\frac{p_i^n - p_{i-1}^n}{\Delta x}\right) - q\delta_{i,k} = \phi_i c_t A\Delta x\left(\frac{p_i^n - p_{i-1}^n}{\Delta t}\right) \tag{10}$$

for $i = 2, 3, \ldots, N-1$ and $= 1, 2, \ldots$. At $i = 1$ and $i = N$, respectively.

Given the cross-sectional area to the flow, rock and fluid properties, the initial pressure and the flow rate, the forward problem is to solve the system of finite-difference equations, i.e., Equation (10) for p_i^n, $i = 1, 2, \ldots, N$, given p_i^{n-1}, $i = 1, 2, \ldots, N$.

Backward modeling

Peaceman (1983) in his paper presented a relation between the pressure in cell to the wellbore pressure by the following formulae:

$$p_1 - p_{wf} = \frac{q\mu}{2\pi h\left(k_x k_y\right)^{\frac{1}{2}}}\ln\left(\frac{r_1}{r_w}\right) \text{ where } r_1 = 0.14\left(\Delta x^2 + \Delta y^2\right)^{\frac{1}{2}} \tag{11}$$

Any inversion problem needs a backward modeling scheme. The backward model matrix is formed based on this reservoir engineering principle that, for an optimal case, the amount of pressure difference in a distance at any time is equal. Applying the backward modeling scheme on a set of pressure difference data will give the inverse of permeability for each cell according to Eq. (11). Solving for permeability is nonlinear and as a result, the inverse of the permeability is considered as the model parameters in the backward modeling scheme. This is indeed the case if the sum of the inverse of the permeabilities of all cells up to cell i is used in the forward model. The backward model equation is readily formed based on the pressure drop (or difference) relation $\Delta p_i^n = \sum_{j=1}^{i}\frac{c_j}{k_j}$ where i is the number of cell (Ertekin et al., 2001). For the problems at hand, the backward model matrix is primarily constructed as in Fig. 12 which is full rank matrix and it neither has model null space vector nor data null space vector. This matrix is formed based on the assumption that the pressure data are available at each cell.

For reservoir simulation purposes, the reservoir is gridded. The grid mesh is shown in Fig. 6a and the gridded gas injection interval is zoomed for in Fig. 6b. The interval is gridded in such a way to make the inversion problem linear, namely, in a sense that all wells fall in the same raw of the grid.

The schematic setting of the problem in hand is shown in Fig. 7. The interval transferring the injected gas is considered as an intact rock unit and this rock unit is discretized for the purpose of fluid flow simulation.

Discussion

In this paper, two general settings are considered and studied: the controlled experiment and the real case. The controlled experiment is designed and studied to evaluate the performance of different inversion methodologies under different data and sensitivity matrix considerations. To be specific, the controlled experiment case is first designed with the assumption that the pressure data are available at all cells. Then, different inversion methodologies are used and tested both to verify the mathematical soundness of the problem setting, i.e. the forward modeling and the backward modeling, and also to discard the inversion methods which do not lead to reliable results even under perfect conditions (i.e. perfect pressure data at all cells). Same scheme of tests are performed for the case of noisy data in order to study the effect of the noise on the inversion procedure. Accordingly, some amount of noise is added to the pressure data to check the performance of the different inversion methods in the presence of noise. Evidently, adding noise to the data makes the controlled experiment more like the real case.

Furthermore, since the real case scenario is rank-deficient, meaning that the pressure data are only available at the well locations, then the rank-deficient sensitivity matrix is formed to invert only for the noisy data available at the well locations. Under such setting, the controlled case problem is just similar to the real case problem except that the permeability values are known at all cells. This setting provides the opportunity to select the best inversion methods which are able to recover reliable permeability models for the real case problem.

Having said the above, for the controlled experiment, the values of porosities and permeabilities are assigned for each cell. The permeability values are selected according to the field data and within a certain range in order to meet the reality of the reservoir. The values of porosity for the control experiment case are the same as in the real case which is depicted in Fig. 4. However, the permeability values for the controlled case are randomly selected as in Fig. 8.

As the fluid properties and rock properties are concerned, for the controlled experiment setting, same information as in the real case scenario is applied except that the injection rate is considered to be 180 RB/D, the viscosity is 0.5 centipoise, and the total compressibility is considered to be 10^{-5}.

Having the above data and properly setting the mathematics of the forward modeling and backward modeling, different states of the controlled experiment are designed and studied as follows.

Controlled experiment setting, case of applying full-rank matrix on perfect data

In this case, the basic structure of the history-matching problem is set by assuming that the pressure data are available for each cell and that the data are noisy-free. Under such considerations, the forward model is run to generate the pressure profiles for all cells as depicted in Fig. 9. The pressure profile for the gas injection well is highlighted as bold dashed blue line in Fig. 9a along with pressure profiles of other cells which are located left side of the injection well. Figure 9b indicates the pressure profiles for the cells located right side of the injection well. Figure 9 gives the sense that mathematical modeling of the forward model is sound. A further evidence for getting confidence about logical mathematics of the forward modeling is the depiction of pressure quantities for all cells at all times in Fig. 10a and the corresponding pressure differences depicted in Fig. 10b. As illustrated, there is a gradual increase in the pressure quantity at well locations by time and there is a gradient for pressure difference by distancing from the injection cell. Moreover, as the theory predicts, for ideal experimental situations, the amount of pressure difference for a specific cell must be the same at all times, which is the case as we see from Fig. 10b.

Further evidence on the soundness of the mathematical setup for the forward modeling is illustrated in Fig. 11. Figure 11a is a time-lapse illustration of the pressure quantities for all cells at all times. As it is evident from this figure, the reservoir pressure is increasing by time; moreover, the pressure at all times is greater for the injection cell and it declines by distance on both sides of the injection cell. Figure 11b is also a 3D depiction of the variation in pressure quantity and pressure difference for the interval of interest at

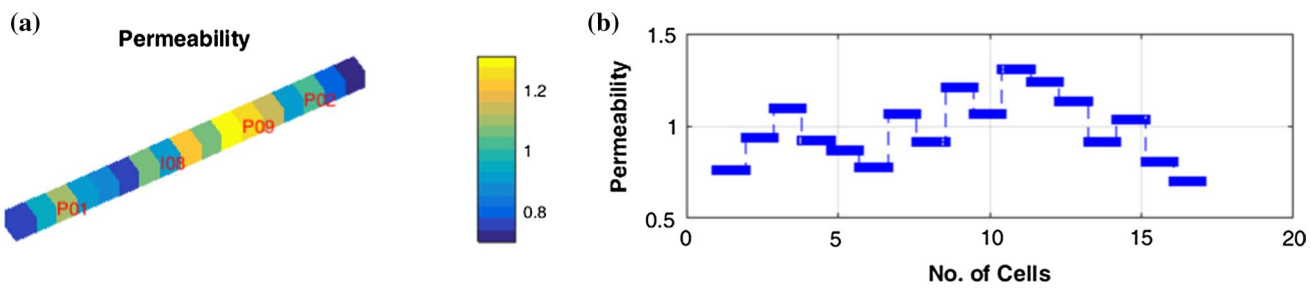


Fig. 8 Permeability profile for the Controlled Experiment; **a** 3D view and **b** plot view

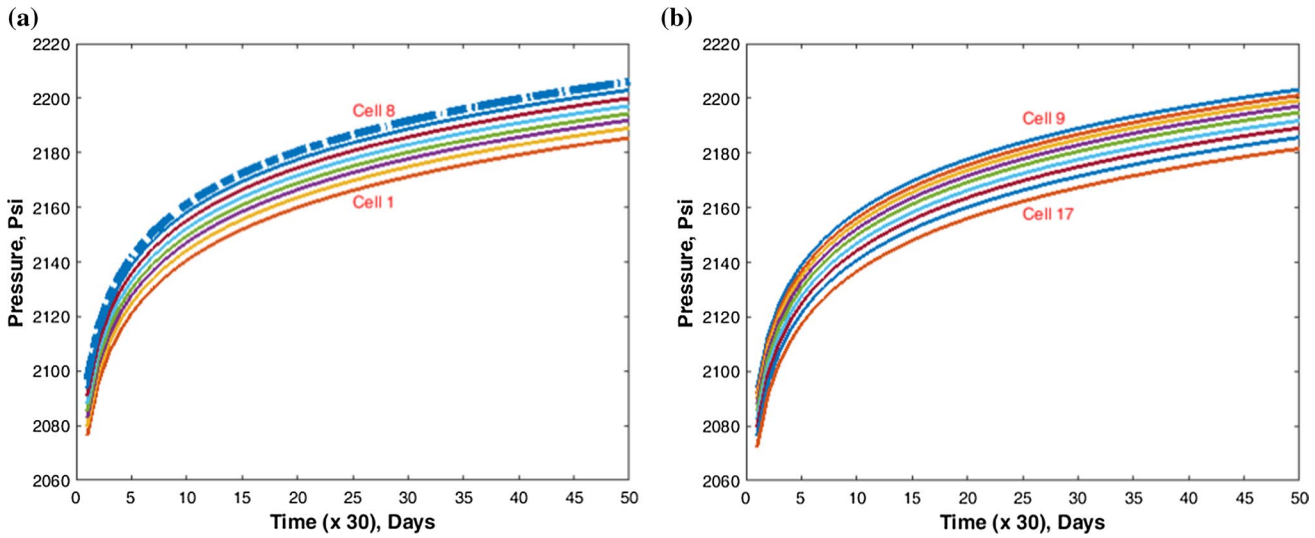


Fig. 9 **a** Pressure profiles for cells number 1 to 8, left side and including the injection well; **b** pressure profiles for cells number 9 to 17, right side of the injection well

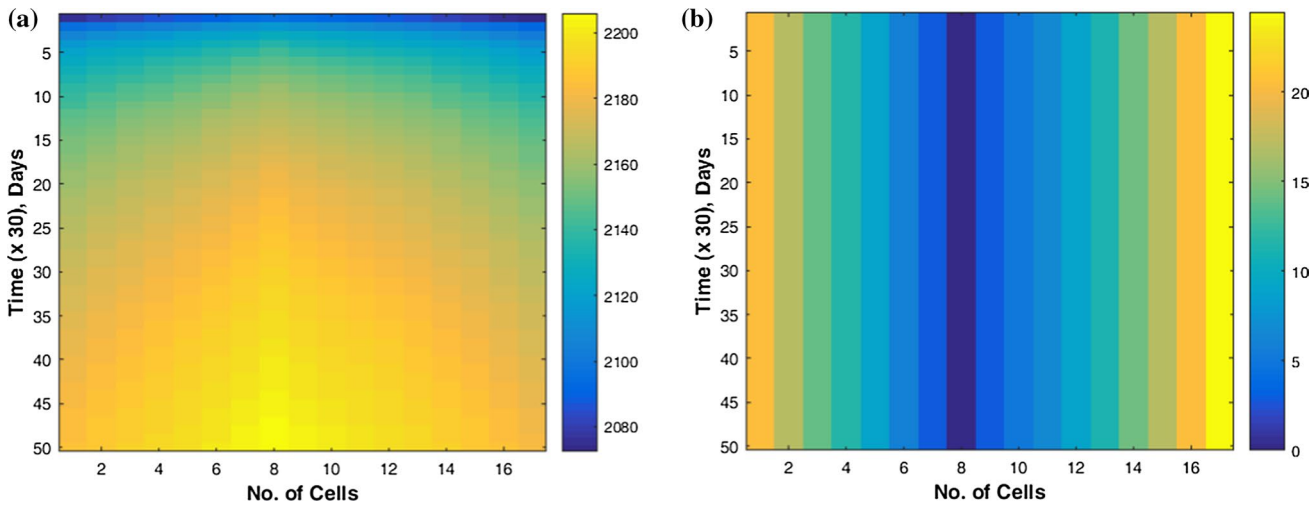


Fig. 10 **a** The modeled pressure quantities for all cell numbers at different times; **b** the modeled pressure difference quantities for each cell at all times

the time of 1500 days. The combination of Figs. 9, 10, and 11 illustrates that the mathematical setting of the forward modeling validates our prior knowledge about reservoir performance for the case of gas injection as posed in this study.

The forward model sensitivity matrix for the controlled experiment case of full-rank type is illustrated in Fig. 12. The columns are scaled by c_j coefficients in the pressure difference formula, i.e. $\Delta p_i^n = \sum_{j=1}^{i} \frac{c_j}{k_j}$, as mentioned under *Backward Modeling* section. In the inversion process, where lots of data corresponding to different times exist, this matrix is augmented accordingly. On the hand, the pressure data should also be augmented to form the augmented data vector, indeed.

Controlled experiment setting, case of applying full-rank matrix on noisy data

As mentioned before, real data always contain some amount of noise which depends on the conditions under which

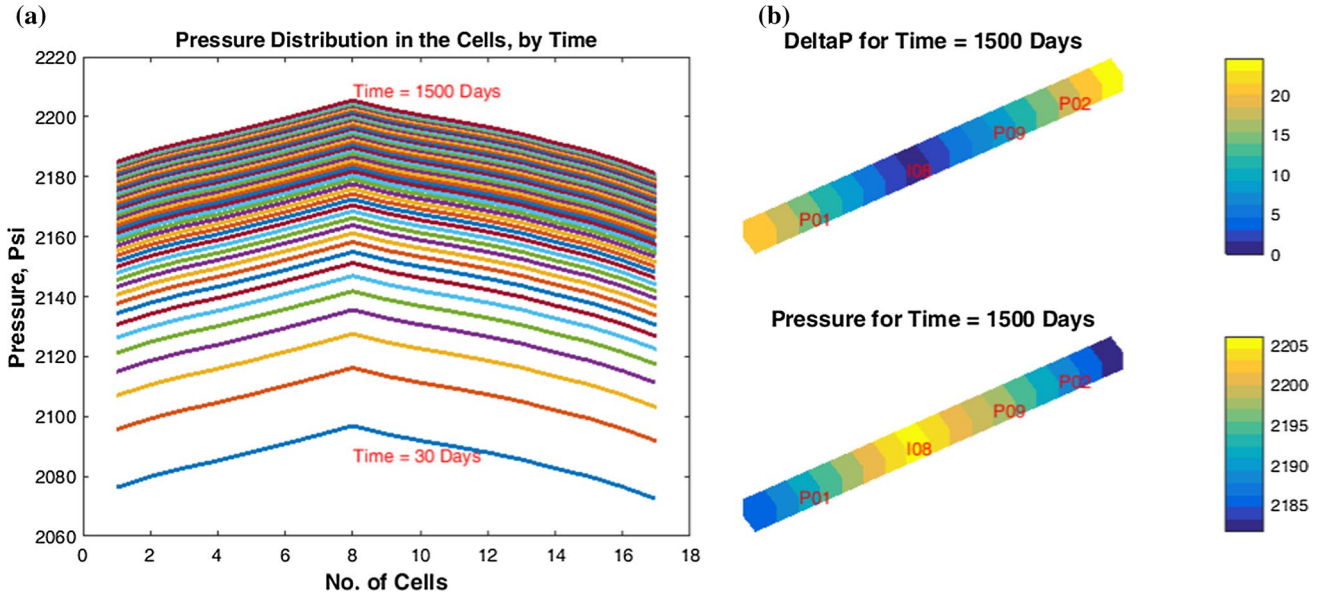


Fig. 11 **a** Time-lapse illustration of the pressure quantities for all cells; **b** 3D illustration of pressure data and pressure difference for the area under study

measurements are discharged. Following this fact, in order to make the controlled experiment more realistic, some noise is added to the modeled pressure quantities to represent the imperfection of the recorded data. Studying the effect of noise on the inversion process and the reconstructed model is a very important step for this study. Observing that some inversion schemes fail to recover perfect permeability models when they are applied on noisy data indicate the sensitiveness of the inversion schemes to the random noise present in the data. At this important step, robust inversion schemes are differentiated from the schemes which are susceptible to the noise.

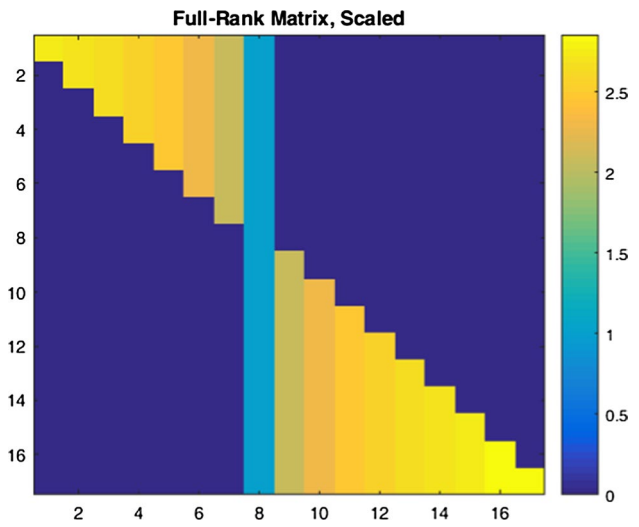


Fig. 12 The full-rank case matrix, where the pressure values are available at each cell

Getting the confidence on the propriety of the mathematical forward modeling from the previous controlled experimental setting, the task at this stage is to add random noise to the pressure data, as depicted in Figs. 13, 14a, and 15a. Correspondingly, the pressure difference data would become noisy as it is illustrated in Figs. 14b and 15b. The results of applying inversion schemes on noisy data are presented under *Results* section.

Controlled experiment setting, case of applying rank deficient matrix on noisy data

Rather than the noise, another very important issue that should be experimented is the effect of rank-deficiency on the inversion results. As mentioned before, the controlled experiment with noisy data and rank-deficient matrix is the most similar state to the real case which should be tested to study the performance and stability of the inversion schemes. The rank-deficient case is the case when the observations are available only at the well locations, i.e. cells No. 3, 8, 12, and 15. Furthermore, for the real case where the distance limits of the pressure data are up to cell No. 3 on the left and cell No. 15 on the right, then cells beyond those limits (which are cells No. 1, 2, 16, and 17) are discarded, because they do not contribute to the fluid flow and that pressure data containing any information of the reservoir properties in those cells are missing. Accordingly, the rank-deficient sensitivity matrix is born from the full-rank sensitivity matrix, Fig. 12, by discarding the rows corresponding to the cells at which real pressure data are not recorded. Based on this, the rank-deficient matrix is represented as in Fig. 16.

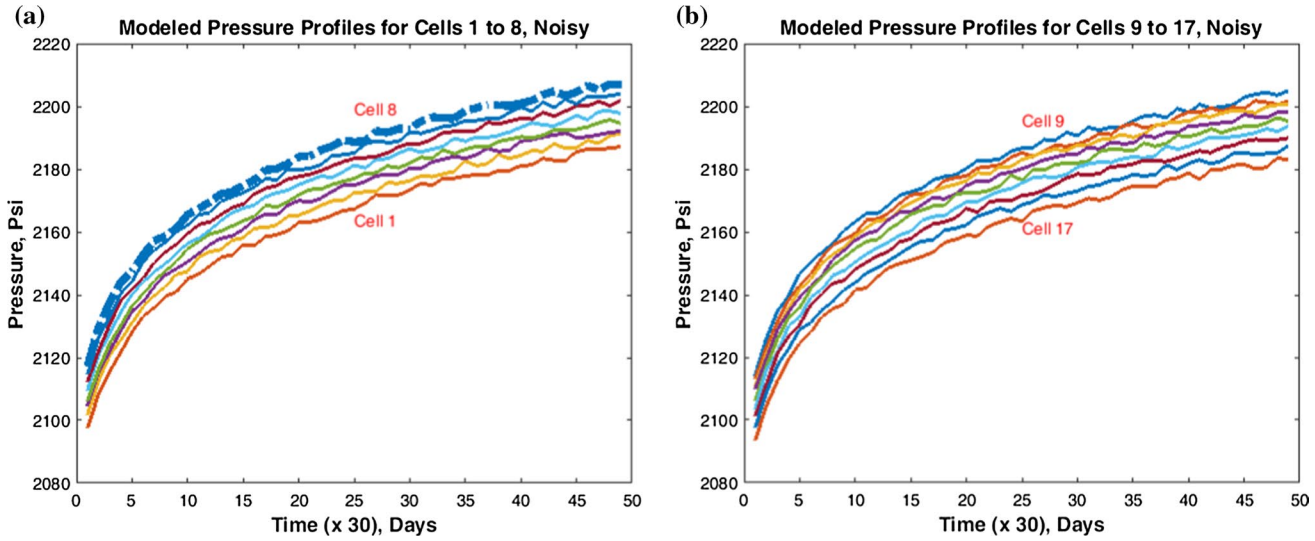


Fig. 13 **a** Noisy pressure profiles for cells number 1 to 8, left side and including the injection well; **b** noisy pressure profiles for cells number 9 to 17, right side of the injection well

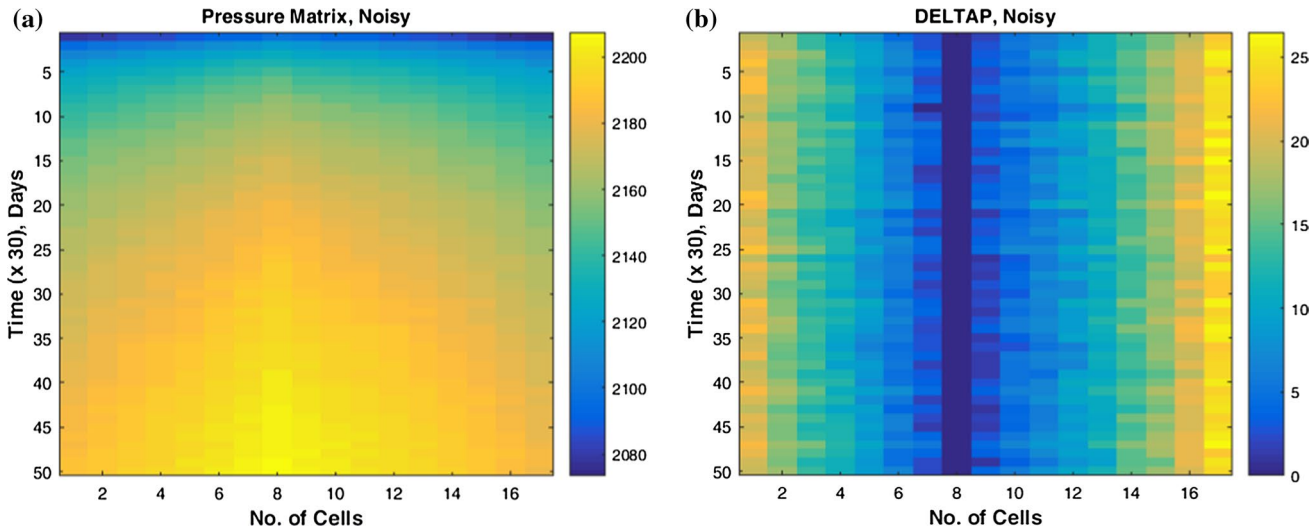


Fig. 14 **a** The noisy modeled pressure quantities for all cell numbers at different times; **b** the noisy modeled pressure difference values for each cell at all times

Results

In this section the results corresponding to the controlled experiments (full-rank sensitivity matrix with perfect data, full-rank sensitivity matrix with noisy data, and rank-deficient sensitivity matrix with noisy data) and the real case are given. The lessons learnt for each section are also presented.

Results for the controlled experiment, case of applying full-rank matrix on perfect data

The controlled experiment with full-rank sensitivity matrix and perfect data is the primitive but optimum way to screen and select best inversion schemes used to reconstruct the permeability model from backward modeling. A dozen of

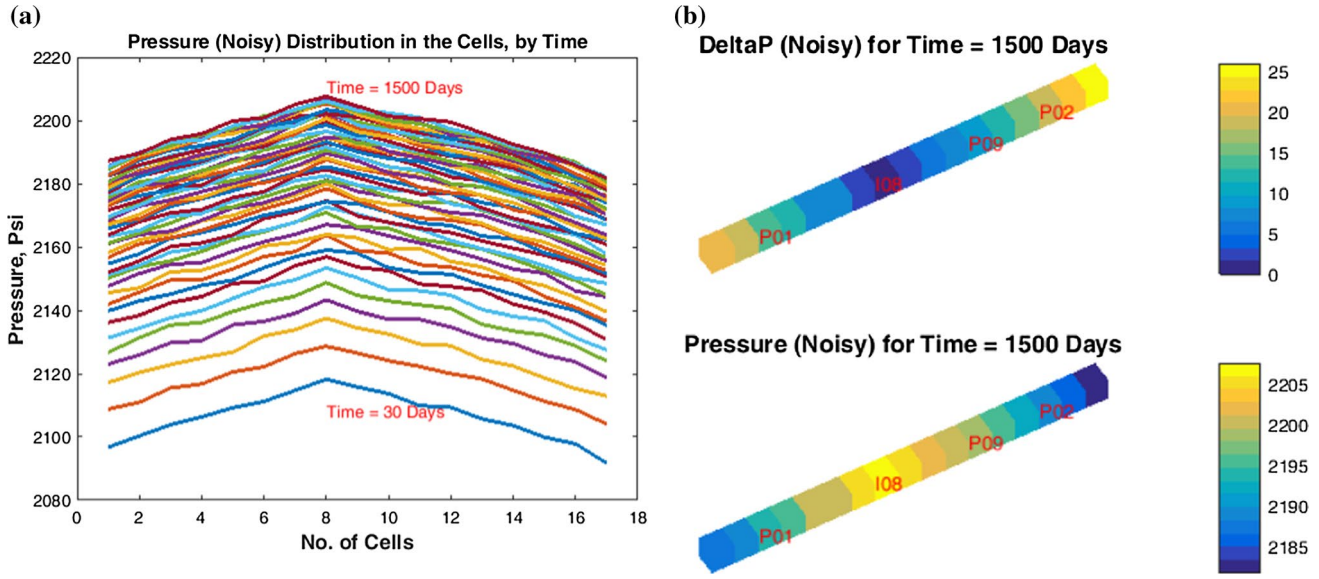


Fig. 15 **a** Time-lapse illustration of the noisy pressure quantities for all cells; **b** 3D illustration of the noisy pressure data and noisy pressure difference

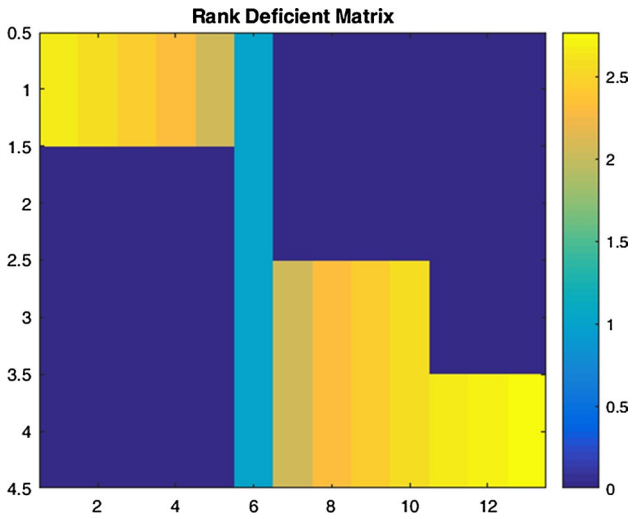


Fig. 16 The rank-deficient case matrix, pressure values are available only at the well locations

inversion schemes are tested at this stage which include truncated singular value decomposition (TSVD), Kaczmarz method, Tikhonov regularization methods (zero-, first-, and second-order), truncated generalized singular value decomposition (TGSVD), conjugate gradient singular value decomposition (CGSVD), generalized cross-validation (CGV), conjugate gradient least squares (CGLS), nonnegative least squares (NNLS), bounded variables least squares (BVLS), maximum entropy, and total variation (TV).

In the case where perfect pressure data are available at each cell, the inversion procedure is perfectly recovering the permeability data using truncated singular value decomposition (TSVD), Kaczmarz method, nonnegative least squares (NNLS), bounded variables least squares (BVLS), maximum entropy, and total variation (TV) methods. Other methods such as Tikhonov regularization (zero-, first-, and second-order) methods and conjugate gradient least squares (CGLS) method were able to recover the permeability model with high precision, although not perfectly. These inversion results ascertain that the mathematical forward modeling and backward modeling work properly.

After careful evaluations of the results obtained from the three proposed states of the controlled experiments (full-rank with perfect data, full-rank with noisy data, and rank-deficient with noisy data), the focus of the discussion of the results are on four inversion methods: second-order Tikhonov regularization method (denoted by 2nd-Tikh), conjugate gradient least squares (CGLS), maximum entropy, and the total variation (TV) methods. This is because, for example, the nonnegative least-squares and the bounded least-squares methods recover the permeability model perfectly when applied to perfect pressure data, however, the results of applying these two methods on the noisy data were completely unsatisfactory.

Following the discussion in the above paragraph, as it is evident in Fig. 17, the maximum entropy and TV methods have perfectly recovered the permeability model. Moreover, the permeability model recovered from the CGLS method is superior to the permeability model recovered from the 2^{nd}-Tikh method. The conclusion from the results of this section would be to consider the maximum entropy and TV methods as the best inversion schemes which can recover the permeability model.

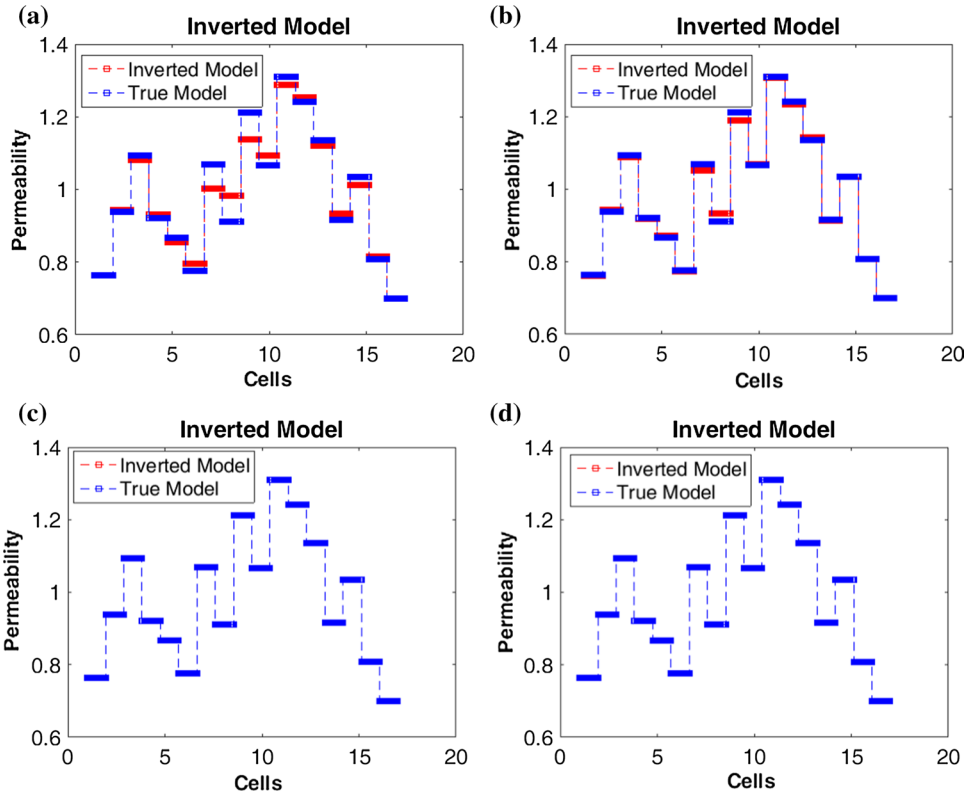


Fig. 17 Controlled experiment, case of full-rank matrix with perfect data; the imperfect reconstruction of the permeability model using **a** 2nd order Tikhonov regularization method and **b** conjugate gradient least squares method. Perfect reconstruction of the permeability model using **c** Maximum Entropy method and **d** Total Variation method

Results for the controlled experiment, case of applying full-rank matrix on noisy data

The controlled experiment for the case of full-rank with noisy data is specifically designed to study the effect of noise on the inversion procedure. Although a full-rank sensitivity matrix is used in the inversion process for this section, the recovered models from all methods are considerably deviated from the true model. The readily conclusion for this section would be that the results are very susceptible to the random noise present in the data.

Another important point to mention is that the deviation of the recovered permeability values from the true model happens for permeability values at the well locations as well. Cells No. 3, 8, 12, and 15 correspond to wells No. 01, 08, 09, and 02, respectively. So far, as in Figs. 12 and 16, the sensitivity matrices are only constrained to the well No. 8 permeability data, which happens naturally. In Fig. 18a and b, which corresponds to 2nd-Tikh and CGLS inversion methods, the permeability value for cell No. 8 is not recovered, whereas in Fig. 18c and d the maximum entropy and the TV inversion methods have perfectly recovered the permeability values for well No. 8. At this time we take the occasion to acknowledge that, again, the maximum entropy and TV methods perform considerably better than the 2nd-Tikh and CGLS methods in recovering the actual data for the known permeability values at the well locations.

Consequently, this brings about the necessity of constraining the inversion procedure to the known permeability values at the other three well-locations corresponding to cells No. 3, 12, and 15. Further studies indicated that such constraining is still necessity even in the case of applying the rank-deficient matrix on the perfect pressure data, because even in this case the true permeability values at the well locations are not recovered (the results are not shown for brevity). As a result, adding more constraints to the system of equations is inevitable. Note that the permeability values at the well locations are known from the well-test data. Augmenting these permeability values into the data vector with corresponding augmentations in the sensitivity matrix, $\boldsymbol{G}$, will apply additional regularization on the system of equations. This is equivalent to conditioning the model with data at well locations which usually arises in geostatistical modeling, e.g., Mariethoz and Caers (2014).

Results for the controlled experiment, case of applying rank-deficient matrix on noisy data

So far, for the case of applying full-rank sensitivity matrix on perfect or noisy data in the backward modeling scheme, all seventeen cells (cells 1 to 17) are included in the inversion process, because the pressure data for all cells exist. However, when the rank-deficient case is considered, the pressure data are only available for the cells which correspond to the

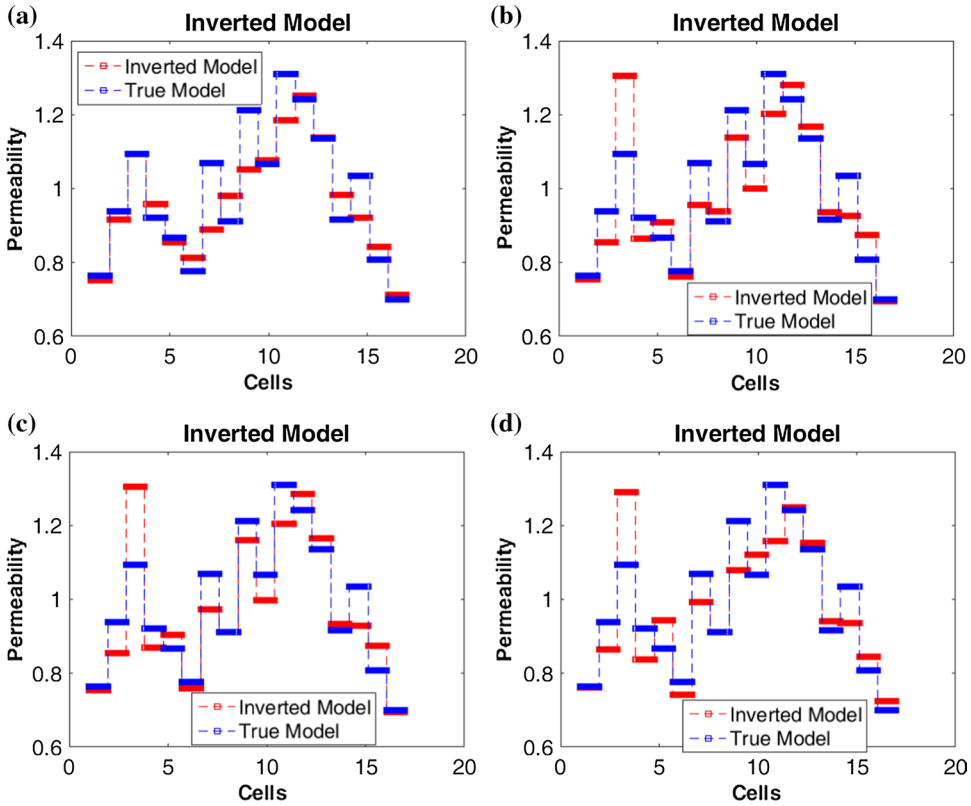


Fig. 18 Controlled experiment, case of full-rank matrix with noisy data; the imperfect reconstruction of the permeability model using **a** 2nd order Tikhonov regularization method, **b** conjugate gradient least squares method, **c** Maximum Entropy method, and **d** Total Variation method

well locations and the cells beyond the distant limits of the wells on both sides of the injection well, are excluded in the backward modeling scheme. This is because there is no pressure data recorded beyond those limits which brings some information on the contribution of those cells to the fluid flow. As a result, cells No. 1 and 2 on the left side and cells No. 16 and 17 on the right side of the gas injection well are excluded and the dimension of the sensitivity matrix for the rank-deficient case is reduced correspondingly.

Having the above said, the forward modeling procedure is run to obtain noisy pressure data as in Figs. 13, 14, and 15. Setting up for the sensitivity matrix and augmenting for the pressure data along with adding constraints for the permeability values at the well locations, the inversion procedure is run. The results of the inversion is represented in Fig. 19. According to this figure, although the expectation is to recover the permeability values at the well locations perfectly, however the 2nd-Tikh method still did not recover the permeability values at the well locations, although the recovered values follow the trend of the true model.

In contrast to the 2nd-Tikh method, the other three methods (CGLS, maximum entropy, and TV) have perfectly recovered the permeability values at the well location . The trend of permeabilities recovered by these methods are also satisfying. To evaluate the performance of these methods in recovering the permeability trend, the chi-squared factor, $\chi^2 = \sum_i \left(m_{esti} - m_{trui}\right)^2$, is calculated for the recovered permeability models. The first two best chi-squared values correspond to maximum entropy and TV methods. The chi-squared values for 2nd-Tikh and CGLS methods are considerably distant from those of the maximum entropy and TV methods. Further experiments were run (not shown for brevity) in order to evaluate this latter observations on the chi-squared values for all four methods. These results further validate that the permeability trend, represented by the chi-squared value, is best recovered by maximum entropy and TV methods and that their chi-squared values are far less comparing to 2nd-Tikh and CGLS methods. The conclusion for this section would be that the maximum entropy and TV methods should both be considered as best candidates to be used for backward modeling the real case data.

Results for the real case

The results obtained from the controlled experiments shed the light on the path to evaluate the results obtained from inversion of the real pressure data. As in the previous cases, four inversion schemes are applied to invert for the pressure data and obtain the permeability model in the area of interest. These results are shown in Fig. 20. In this figure, two criteria are used to evaluate the quality of the inferred permeability models. As the first criteria, the permeability values at the well locations should be perfectly recovered by the inversion methods, as discussed in the controlled

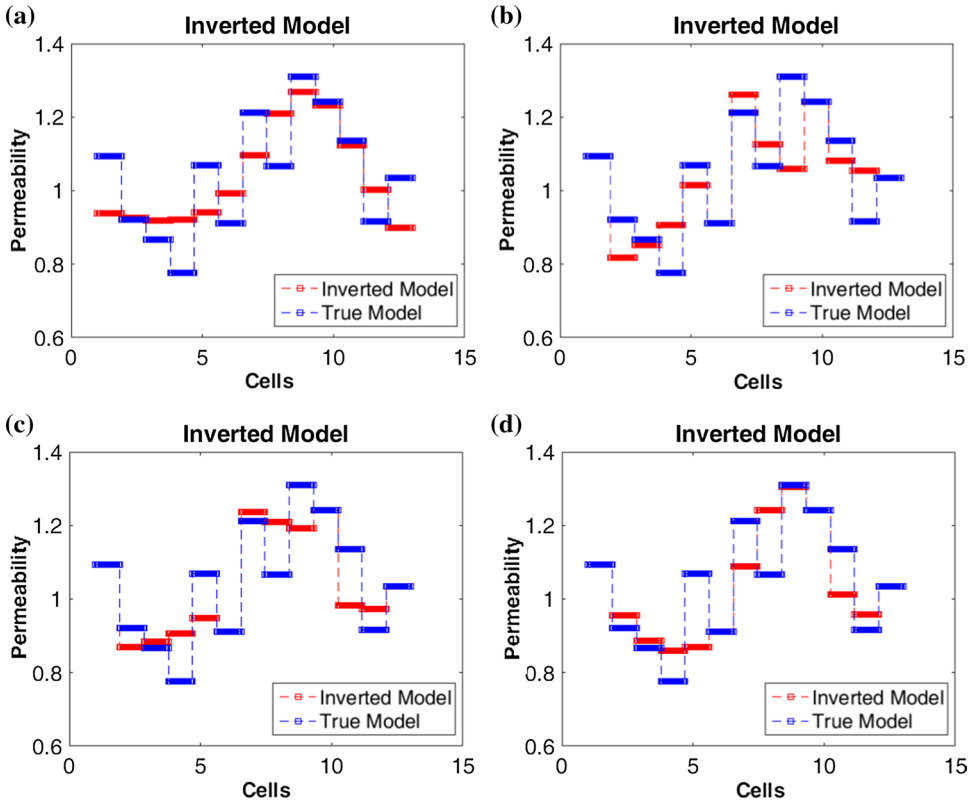


Fig. 19 Controlled experiment, case of rank-deficient matrix with noisy data; the imperfect reconstruction of the permeability model using **a** 2nd order Tikhonov regularization method with Chi2 = 0.1322, **b** conjugate gradient least squares method with Chi2 = 0.1218, **c** Maximum Entropy method with Chi2 = 0.0957, and **d** Total Variation method with Chi2 = 0.1113

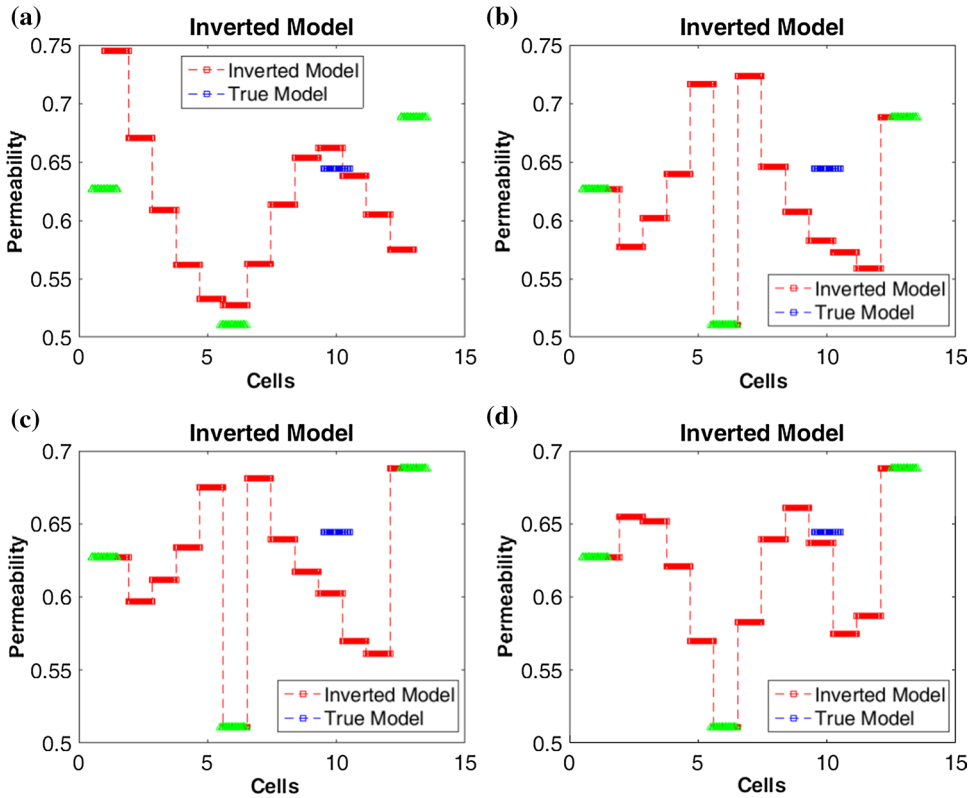


Fig. 20 Reconstructed permeability models for the real case by applying **a** 2nd order Tikhonov regularization method, **b** conjugate gradient least squares method, **c** Maximum Entropy method, and **d** Total Variation method

experiment case of applying the rank-deficient on noisy data. Furthermore, since in the real case the advantage of using the chi-squared criteria is missing (because the true model is unknown), as a result the inversion procedure is constrained only to true permeability values at locations of wells No. 01, 08, and 02. This means that the value of the true permeability for well No. 09 is left out of the inversion procedure in order to evaluate the quality of the inversion results. Such an approach is a common practice in seismic inversion methods, as also applied in the original paper by Hosseini and Riahi (2019b) resulted in detecting the gas-fingering event depicted in Fig. 2.

Having that said, the results represented in Fig. 20 are now interpreted. The red-colored response corresponds to the inverted permeability models. The green-colored values correspond to the true permeability values at the locations of wells No. 01, 08, and 02. The blue-colored value corresponds to the true permeability value at location of well No. 09 which is left out of the inversion procedure for evaluating the quality of inverted permeability model. Accordingly, as it is evident from Fig. 20, the inverted permeability model using 2nd-Tikh method has not acknowledged the true permeability values at any locations of wells No. 01, 08, and 02, despite the fact that these values are assigned to the inversion process as constraints. This was also the case as we witnessed from the controlled experiment case of applying the rank-deficient matrix on noisy data. The other three inversion methods (namely, CGLS, Max. Ent., and TV) were successful in recovering the permeability values at the well locations which are used as constraints in the inversion procedure.

Therefore, in order to discriminate between the inverted models obtained by applying the CGLS, maximum entropy, and TV methods as the backward modeling scheme, one should consider the inverted model quality for the unassigned permeability value at the location of well No. 09. We already learned from the case of applying the rank-deficient matrix on noisy data that performance of the maximum entropy and TV methods in recovering the permeability models are superior to the CGLS method. Comparing the results in Fig. 20b with the results in Fig. 20c, d indicates that the permeability value for well No. 09, which was excluded from the inversion procedure, is poorly recovered (i.e., more distant) by using the CGLS method, as compared to maximum entropy and TV methods. This is in accordance with the lessons learnt from the controlled experiment of applying the case rank-deficient matrix on noisy data.

Comparing the results of having maximum entropy (as in Fig. 20c) and TV (as in Fig. 20d) methods as the inversion approaches, the total variation method as compared to the maximum entropy and other methods applied in this paper, has been able to correctly reconstruct the permeability values for well No. 9 which was excluded from the inversion procedure. Furthermore, referring to the lessons learnt from the controlled experiment case of applying the rank-deficient matrix on noisy data, we had found that the total variation method along with the maximum entropy method are the two best inversion schemes for reconstructing the permeability model. These observations lead us to the conclusion that the recovered permeability model, considering both the acknowledgement of the data at the well locations and the trend inherent therein (which is evaluated by closely estimating the permeability value of the excluded well), is possibly the best model that can be proposed to reconstruct the permeability model for the real case problem.

We should emphasize that the task of inferring reservoir properties from the fluid flow data is a highly nonlinear problem and accordingly, many permeability models, in the form $\boldsymbol{m} + \boldsymbol{m}_0$ ($\boldsymbol{m}$: the inferred solution and $\boldsymbol{m}_0$: model from the null space), might satisfy in the system of equations and lead to the same set of observation.

An estimation for the permeablity of fractures

The inverted permeability model is thought to represent the permeability of the intact reservoir rock, which is a combination of matrix and fracture permeabilities. Estimation of the fracture permeability for each cell block is not straightforward in this case. One assumption that has to be made for such a purpose is to consider the parallel model for the fracture-matrix mediums. In such a case, the total permeability, k_t, is related to matrix permeability, k_m, and fracture permeability, k_f, as follows

$$\frac{1}{k_t} = \frac{1}{k_m} + \frac{1}{k_f} \tag{12}$$

For the problem at hand, k_t is known and it is the inverted permeability model, whereas the other two parameters are unknown. However, a correlation can be obtained for the porosity values versus matrix permeability values if core data for the interval under investigation is available.

Based on such an approach, a set of core porosity–permeability data for the interval of interest were collected for the oil field under study and two other adjacent oil fields. This is because the number of core data available for the oil field under study were seldom. The data are plotted in Fig. 21 along with the error bars.

The best correlation line along with upper and lower limits of 95% confidence interval are also plotted on Fig. 21. Note that the y-axis is in logarithmic scale. Because we are dealing with a set of data, the uncertainty inherent in the data should also be dealt with and that is why an interval of 95% confidence is studied in order to obtain upper and lower limits for the fracture permeabilities for each cell.

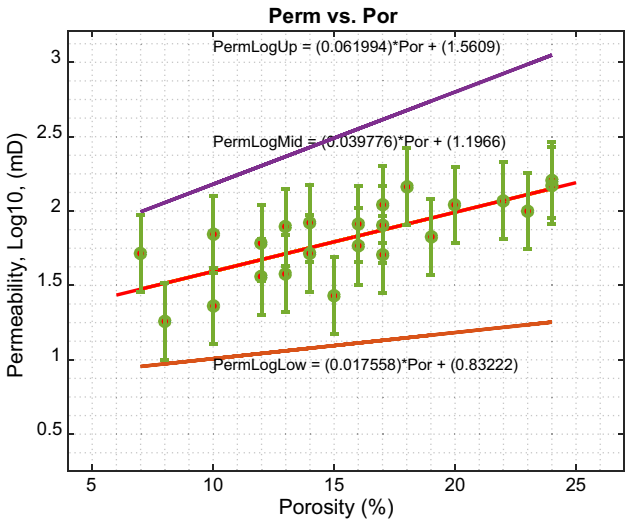


Fig. 21 Core porosity–permeability data for the interval of interest

According to the upper, middle, and lower correlations for the porosity–permeability plot, matrix permeability values corresponding to each cell are obtained, as the porosity values for each cell are known from the inversion of seismic data. The estimated matrix permeability is plotted in Fig. 22a using the correlations indicated in Fig. 21. In this figure, three permeability values are estimated corresponding to lower limit, best case (or middle), and upper limit correlations. Furthermore, the fracture permeability values estimated using Eq. 12 are also plotted in Fig. 22b. This figure indicates that the total permeability is dragged toward the lower limit of the fracture permeabilities. This is in fact due to the effect of the matrix permeability which in parallel with the fracture permeability results in a total permeability closer to the lower limit of the estimated fracture permeability.

Figure 23 is another depiction of the status of the total permeability, best case matrix permeability, and best case fracture permeability. This figure indicates that the total permeability is very much representing the fracture permeability rather than the matrix permeability which is usually the case in naturally fractured reservoirs. Meanwhile, as emphasized in the interpretations of Fig. 22, the act of matrix permeability on the total permeability is that the total permeability is dragged just below the best case fracture permeability.

Conclusions

In order to estimate the permeability model of an area where a gas-fingering event is observed, the forward and backward modeling procedures were set up and the modeled data were evaluated to validate the soundness of the mathematical setting of the forward modeling.

The backward modeling procedure is performed using a dozen of inversion schemes. All of these schemes are applied and studied in all cases of the controlled experiment. The studies lead to recognition of four inversion schemes as main inversion methods in order to continue the study with and eventually use them for the inversion of the real data. The four selected inversion schemes were the second-order Tikhonov regularization method, conjugate gradient least

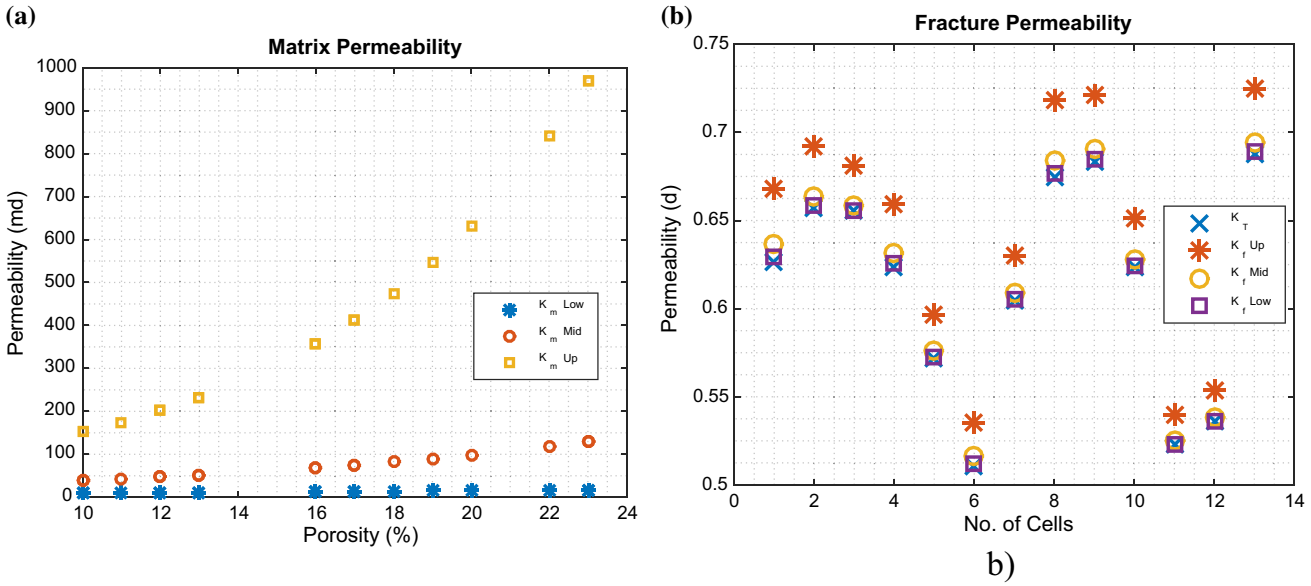


Fig. 22 **a** The estimated matrix permeability; **b** the estimated fracture permeability

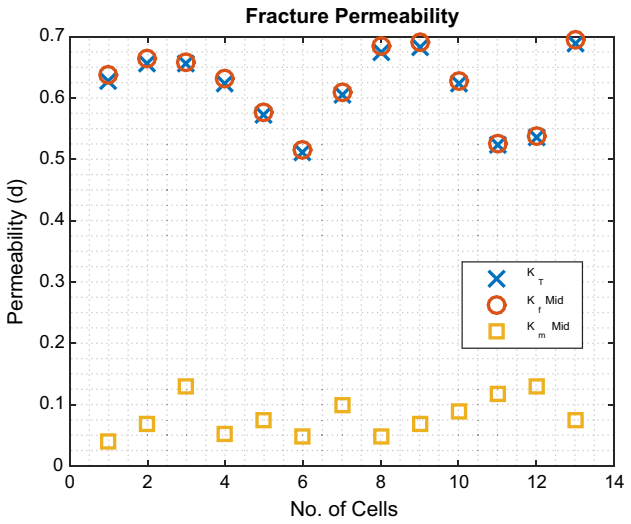


Fig. 23 The comparison of the total permeability, with the best case matrix and fracture permeability

squares algorithm, maximum entropy, and total variation methods.

Further experiments necessitated the utilization of the permeability values at the well locations as further constraints for the inversion process. Having such a modification applied on the inversion process, the controlled experiment case of applying the rank-deficient on noisy data was designed to study the results of the performance of the four inversion schemes, i.e., 2nd-Tikh, CGLS, maximum entropy, and TV. These results which were supported by quantitative measurements using the chi-squared criteria, revealed that the maximum entropy and the TV approaches are the best methods to recover the true permeability model among the selected four schemes.

For the real case, the four inversion schemes (i.e., 2nd-Tikh, CGLS, maximum entropy, and TV) were applied on the real data and the results were evaluated. These results indicated that the CGLS, maximum entropy, and TV methods are able to acknowledge the permeability values at the well locations. Excluding one of the wells out of the inversion procedure as constraint and checking for the quality of the inversion schemes in reconstructing the permeability value at this location (i.e., well No. 09), the results indicated that the total variation method is able to give the best estimation of the permeability value for the well excluded from the inversion procedure.

An attempt was also made to estimate the fracture permeabilities from the inverted permeability model. The result of such study revealed that the inverted total permeability values are in fact representing quantities of the fracture permeabilities and that the matrix permeabilities fall far below such values.

Acknowledgement This study did not receive fund from any institution or non-for-profit organizations. It is designed and experimented by the author; however, he would like to thank the Geology and Geophysics department of the National Iranian South Oil Company and also the Reservoir Engineering department of the same oil company.

Declarations

Conflict of interest The author declares no conflict of interest.

References

Aanonsen SI, Tveit S, Alerini M (2019) Using Bayesian Model Probability for Ranking Different Prior Scenarios in Reservoir History Matching, SPE-194505-PA, SPE Journal, 24(4). https://doi.org/https://doi.org/10.2118/194505-PA.

Aster RC, Borchers B, Thurber CH (2005) Parameter estimation and inverse problems. Elsevier, Boston

Caers J, Hoffman T (2006) The probability perturbation method: a new look at Bayesian inverse modeling. Math Geol 38(1):81–100

Chakra NC, Saraf DN (2016) History matching of petroleum reservoirs employing adaptive genetic algorithm. J Pet Explor Prod Technol 6(4):653–674

Chen Y, Oliver DS (2013) Levenberg–Marquardt forms of the iterative ensemble smoother for efficient history matching and uncertainty quantification. Comput Geosci 17:689–703. https://doi.org/10.1007/s10596-013-9351-5

Cominelli A, Ferdinandi F, de Montleau PC, Rossi R (2007) Using gradients to refine parameterization in field-case history-matching projects. SPE Reserv Evalu Eng 10(3):233–240

dos Santos Amorim EP, Goldfeld P, Dickstein F, dos Santos RW, Xavier CR (2010) Automatic History Matching in Petroleum Reservoirs Using the TSVD Method. In: Taniar, D., Gervasi, O., Murgante, B., Pardede, E., Apduhan, B.O. (eds.) ICCSA 2010. LNCS, vol. 6017, pp. 475–487. Springer, Heidelberg.

Efendiev Y, Hou T, Luo W (2006) Preconditioning Markov chain Monte Carlo simulations using coarse-scale models. SIAM J Sci Comput 28(2):776–803

Emerick AA, Reynolds AC (2011) History matching a field case using the ensemble kalman filter with covariance localization. SPE Res Eval Eng 14(4):443–452. https://doi.org/10.2118/141216-PA

Ertekin T, Abou-Kassem JH, King GR. Basic Applied Reservoir Simulation, SPE Textbook Series, Vol. 7.

Evensen G. (2009) Data Assimilation the Ensemble Kalman Filter, Springer-Verlag Berlin Heidelberg, 2nd edition, https://doi.org/10.1007/978-3-642-03711-5.

Eydinov D, Aanonsen SI, Haukas J, Aavatsmark I (2008) A method for automatic history matching of a compositional reservoir simulator with multipoint flux approximation. Comput Geosci 12(2):209–225

Gao G, Vink JC, Chen C, El Khamra Y, Tarrahi MA (2017a) Distributed gauss-newton method for history matching problems with multiple best matches. Comput Geosci 21(5–6):1325–1342. https://doi.org/10.1007/s10596-017-9657-9

Gao G, Jiang H, Hagen PV, Vink J, Wells T (2017) A Gauss–Newton Trust Region Solver for Large-Scale History Matching Problems, Presented at the SPE Reservoir Simulation Conference, Montgomery, Texas, SPE-182602-MS. https://doi.org/https://doi.org/10.2118/182602-MS.

González-Rodríguez P, Kindelan M, Moscoso M, Dorn O (2005) History matching problem in reservoir engineering using the propagation-backpropagation method. Inverse Probl 21:565–590

Hosseini M, Riahi MA (2019) Using input-adaptive dictionaries trained by the method of optimal directions to estimate the permeability model of a reservoir. J Appl Geophys 165:16–28. https://doi.org/10.1016/j.jappgeo.2019.04.006

Hosseini M, Riahi MA (2019) Detecting a gas injection front using a 3D seismic data: case of an Asmari carbonate reservoir in the Zagros basin. Carbonates Evaporites 34:1657–1668. https://doi.org/10.1007/s13146-019-00514-2

Jo H, Jung H, Ahn J, Lee K, Choe J (2017) History matching of channel reservoirs using ensemble Kalman filter with continuous update of channel information. Energy Explor Exploit 35(1):3–23

Kazemi A, Stephen KD (2013) Optimal parameter updating in assisted history matching using streamlines as a guide. Oil Gas Sci Technol 68(3):577–594. https://doi.org/10.2516/ogst/2012071

Kazemi A, Stephen KD (2012) Schemes for automatic history matching of reservoir modeling: a case of nelson oilfield in UK. Petrol Explor Dev 39(3):349–361. https://doi.org/10.1016/S1876-3804(12)60051-2

Kreyszig E (2017) Advanced Engineering Mathematics, 10th edition, Wiley publication.

Li R, Reynolds AC, Oliver DS (2003) Sensitivity coefficients for three-phase flow history matching. J Can Pet Technol 42(4):70–77

Liao Q, Zeng L, Chang H, Zhang D (2019) Efficient History Matching Using the Markov-Chain Monte Carlo Method by Means of the Transformed Adaptive Stochastic Collocation Method, SPE-194488-PA, SPE Journal, Volume 24, Issue 04, https://doi.org/https://doi.org/10.2118/194488-PA.

Mariethoz M, Caers J (2014) Multiple-point geostatistics: stochastic modeling with training images. John Wiley and Sons Ltd. https://doi.org/10.1002/9781118662953

Maschio C, Schiozer DJ (2008) A New Methodology for assisted history matching using independent objective functions. Pet Sci Technol 26(9):1047–1062. https://doi.org/10.1080/10916460701208389

Olalotiti-Lawal F, Datta-Gupta A (2018) A multiobjective markov chain monte carlo approach for history matching and uncertainty quantification. J Pet Sci Eng 166(July):759–777. https://doi.org/10.1016/j.petrol.2018.03.062

Oliver DS, Reynolds AC, Liu N (2008) Inverse theory for petroleum reservoir characterization and history matching, 1st editon. Cambridge University Press, Cambridge

Onwuchekwa C, Dennar L, Ahmed S, Bakare O, and Emelle C (2017) Adjoint-Based Assisted History Matching: A Niger Delta Field Case Study. Paper SPE-189155-MS presented at the SPE Nigeria Annual International Conference and Exhibition held in Lagos, Nigeria, 31 July – 2 August.

Oyerinde A, Datta-Gupta A, Milliken W (2009) Experiences with streamline-based three-phase history matching. SPE 109964, SPE Reserv. Evalu. Eng. 12(4), 528–541.

Peaceman DW (1983) Interpretation of well-block pressures in numerical reservoir simulation with non-square grid blocks and anisotropic permeability, SPE. Trans AIME 275:10–22

Quarteroni A, Sacco R, Saleri F (2007) Numerical mathematics, 2nd edn. Springer-Verlag, Berlin Heidelberg

Raghu A, Yang X, Khare S, Prakash J, Huang B, Prasad V (2017) Reservoir history matching using constrained ensemble Kalman filtering. Can J Chem Eng. https://doi.org/10.1002/cjce.22965

Rodrigues JRP (2006) Calculating derivatives for automatic history matching. Comput Geosci 10(1):119–136

Romary T (2009) Integrating production data under uncertainty by parallel interacting Markov chains on a reduced dimensional space. Comput Geosci 13(1):103–122

Romero CE, Carter JN (2001) Using genetic algorithms for reservoir characterisation. J Pet Sci Eng 31(2–4):113–123

Stenerud VR, Kippe V, Lie KA, Datta-Gupta A (2008) Adaptive multiscale streamline simulation and inversion for high-resolution geomodels. SPE J 13(1):99–111

Zhang X, Awotunde AA (2016) Improvement of Levenberg-Marquardt algorithm during history fitting for reservoir simulation. Pet Explor Dev 43(5):876–885. https://doi.org/10.1016/S1876-3804(16)30105-7